Received: 21 November 2023 | Revised: 6 March 2024 | Accepted: 17 March 2024

DOI: 10.1002/cbin.12163

RESEARCH ARTICLE

Cell Biology International WILEY

L-kynurenine and quinolinic acid inhibited markers of cell survival in B16 F10 melanoma cells in vitro

Charlise Basson[1] | June Cheptoo Serem[2] | Priyesh Bipath[1] | Yvette Nkondo Hlophe[1]

[1]Department of Physiology, School of Medicine, University of Pretoria, Pretoria, South Africa

[2]Department of Anatomy, School of Medicine, University of Pretoria, Pretoria, South Africa

Correspondence
Yvette Nkondo Hlophe, Department of Physiology, Faculty of Health Sciences, School of Medicine, University of Pretoria, Private Bag X323, Gezina, Pretoria Gauteng 0031, South Africa.
Email: yvette.hlophe@up.ac.za

Funding information
National Research Foundation, Grant/Award Numbers: A15685, N15580; Struwig-Germeshuysen Kankernavorsingstrust; RESCOM; RDP, Grant/Award Numbers: A1B521, A1B523

Abstract

Melanoma is an aggressive malignancy and remains a major cause of skin cancer mortality, highlighting the need for new treatment strategies. Recent findings revealed that L-kynurenine and quinolinic acid induce cytotoxicity and morphological changes in B16 F10 melanoma cells in vitro. This paper highlights the effects of L-kynurenine and quinolinic acid at previously determined half-maximal inhibitory concentrations on cell cycle progression, cell death and extracellular signal-regulated protein kinase inhibition. Melanoma, B16 F10 and murine macrophages, RAW 264.7 cells were used in this study, as both cell lines express all the enzymes associated with the kynurenine pathway. Post exposure to the compounds at half-maximal inhibitory concentrations, transmission electron microscopy was used to assess intracellular morphological changes. Flow cytometry was used to analyse cell cycle progression and quantify apoptosis via the dual staining of Annexin V and propidium iodide and cell survival via extracellular signal-regulated protein kinase. L-kynurenine and quinolinic acid at half-maximal inhibitory concentrations induced intracellular morphological changes representative of cell death. Flow cytometry revealed alterations in cell cycle distribution, increased apoptosis and significantly inhibition of cell survival. L-kynurenine and quinolinic acid are exogenous kynurenine compounds which inhibited cell survival through extracellular signal-regulated protein kinase inhibition, induced cell cycle alterations and induced apoptosis in B16 F10 melanoma cells.

KEYWORDS
apoptosis, cancer, kynurenine metabolites, melanoma, survival

1 | INTRODUCTION

Melanoma, resulting from the mutation of pigment-producing cells namely melanocytes (Domingues et al., 2018; Rebecca et al., 2020), is an aggressive malignancy and remains a major cause of skin cancer mortality. As such, it contributes to approximately 80% of skin cancer-related deaths worldwide (Dhanyamraju & Patel, 2022). The alarming rise in incidence and mortality demonstrates the urgency for new treatment strategies (Guan et al., 2021). However, treatment failure is typically caused by metastasis (Leonardi et al., 2018), which

involves a multistep process whereby tumour cells invade the surrounding tissue, migrate into the blood or lymphatic circulatory system in a process known as intravasation and extravasate at the secondary site, where they adhere and proliferate (van Zijl et al., 2011). As such, the typical hallmarks of cancer include evading growth suppressors, resisting cell death, enabling replicative immortality and sustained proliferative signalling (Hanahan & Weinberg, 2011). The uncontrolled cell proliferation in cancer is promoted by impaired cell cycle regulation and deregulated cell death (Zhivotovsky & Orrenius, 2010). It is well known that deregulated cell death is often promoted by hyperactivated oncogenic signalling pathways in cancer (Sever & Brugge, 2015). One of these pathways includes the mitogen-activated protein kinase (MAP-K) pathway, which comprises four subpathways, including the extracellular signal-regulated kinase 1/2 (ERK1/2) cascade. Furthermore, ERK1/2 phosphorylation is associated with cell differentiation, survival and proliferation (Nkandeu et al., 2022).

Although decades of research contributed to the advancement of knowledge regarding new treatments to combat cancer and alleviate critical side effects, metastatic melanoma has evaded all attempts at treatment (Davis et al., 2019). Recently, it has been reported that kynurenine compounds, namely L-kynurenine (L-kyn) and quinolinic acid (Quin) induced cytotoxicity and subcellular morphological changes in B16 F10 melanoma cells at half-maximal inhibitory concentration (IC_{50}) after 48 h in vitro (Basson et al., 2023b). Biologically active kynurenine metabolites are formed through tryptophan catabolism via the kynurenine pathway (Macchiarulo et al., 2009), namely due to insufficient dietary niacin consumption or in immunomodulatory conditions, such as cancer (Basson et al., 2023a; Mehmel et al., 2020; Moffett et al., 2020).

The kynurenine pathway allows for NAD^+ production, which is a cofactor and may support the energy requirements of cancer cells to sustain uncontrolled proliferation (Moffett & Namboodiri, 2003; Navas & Carnero, 2021). Overall, kynurenine metabolites have been reported to exert effects on a multitude of physiological processes while demonstrating implications in carcinogenesis and metastasis. Notably, L-kyn, the central metabolite in the kynurenine pathway, has previously been identified as a potent cytotoxic compound against B16 F10 melanoma cells, surpassing the effects of Quin, an end metabolite in the same pathway (Basson et al., 2023b). However, activated downstream signalling pathways, such as aryl hydrocarbon receptors (Ahr) activation resulting from L-kyn (an AhR agonist), previously induced contrasting biological effects in different cancers, yielding pro- and anticancerous effects (Bungsu et al., 2021; Nkandeu et al., 2022). Given the contradictory impact of kynurenine metabolites on cancer progression, there is a critical need to elucidate the specific roles of these metabolites in the intricate pathways of melanoma carcinogenesis and metastasis. In light of these considerations, the aim of this study is to investigate the effects of L-kyn and Quin at IC_{50} on cell cycle progression, cell death (apoptosis and necrosis) and ERK1/2 inhibition. By investigating the potential nuanced effects of kynurenine metabolites, this research aims to provide insights to guide targeted treatments for melanoma.

2 | METHODS

2.1 | Cell lines

The melanoma (B16 F10) cell line is characterised as a standard cell line for melanoma research and was previously used to determine the IC_{50} values, which were used in this study (Basson et al., 2023b). The B16 F10 cell line was purchased from the American Type Culture Collection B16 F10 (ATCC® CRL-6475™) and used between passages 4-12. The RAW 264.7 cell line is a noncancerous, macrophage-like cell line and was used as the control cell line, as macrophages are known to express all the enzymes associated with the kynurenine pathway (Guillemin et al., 2003). This cell line was purchased from CELLONEX and used between passages 6–20.

2.2 | Sample preparation

The selection of concentrations for this study was informed by a preceding study wherein the IC_{50} values of these metabolites were determined through the employment of a crystal violet assay, spanning a concentration range extending from 0 to 5 mM. As such, all compounds were prepared to IC_{50} concentrations as previously determined, where L-kyn had an IC_{50} of 1.74 mM and Quin acid 8.23 mM at 48 h in B16 F10 melanoma cells (Basson et al., 2023b). Briefly, L-kyn, Quin and nocodazole (NOC) (a microtubule inhibitor used as a positive control) were dissolved in ≤0.1% volume per volume (v/v) dimethyl sulfoxide and diluted in 0.1 M phosphate-buffered saline (PBS). Positive control cells were exposed to 1.30 mM NOC diluted in ddH_2O. A vehicle control sample of complete culture medium (CCM) and PBS in a 1:1 ratio was included as PBS serves as the diluent for L-kyn and Quin. Similarly, a CCM:ddH_2O vehicle control was included, as ddH_2O acts as the diluent for NOC. This approach aligns with the methodology of a prior study (Basson et al., 2023b).

2.3 | General culture maintenance

Cells were cultured in sterile culture flasks in CCM, containing Dulbecco's modified essential medium, 10% foetal calf serum and 1% antibiotics (amphotericin/penicillin/streptomycin) in a humidified atmosphere at 37°C with 5% CO_2 in a Forma Scientific water-jacketed incubator. To detach and plate cells, B16 F10 cells were trypsinised with TrypLE™ Express whereas RAW 264.7 cells were scraped and resuspended in 1 mL of CCM and counted.

2.4 | Transmission electron microscopy

A volume of 4.5 mL at a concentration of 20×10^4 B16 F10 and RAW 264.7 cells/mL was plated in a T25 cm^2 tissue culture flask (9×10^5 cells/flask). B16 F10 and RAW 264.7 cells were treated at stated IC_{50} values (Section 2.2). After 48 h the cells were harvested, and cell suspensions

were washed with 0.1 M PBS. All washes included centrifugation at 3000 rpm. The cells were then fixed with 2.5% glutaraldehyde/formaldehyde solution for 1 h, then washed three times with 0.1 M PBS for 10 min. One millilitre of osmium tetroxide solution (1%) was then added for 1 h to the cells, followed by washing three times with 0.1 M PBS for 10 min each and then cells were consecutively dehydrated with 30%, 50%, 70%, 90% and three times with 100% ethanol (10 min each). After dehydration, the cell pellet was suspended in propylene oxide for 10 min and then suspended in a 2:1 mixture of propylene oxide and epoxy resin for 1 h in an angled rotator. The samples were then suspended in a 1:2 mixture of propylene oxide and epoxy resin overnight in an angled rotator. The pellet was then set in a mould with 100% epoxy resin in a microcentrifuge tube and placed in an oven at 65°C for 36 h. The moulds were then trimmed and sectioned into ultrathin sections with glass and then with a diamond knife, using a microtome. The samples were then stained in urinyl acetate for 5 min and then washed three times in ddH_2O. Samples were then stained with lead citrate for 2 min, followed by three times washes in ddH_2O. A paper filter was then used to blot samples and dried before viewing them with a transmission electron microscope (JOEL JEM-2100F, 200 kV FE (Field Emission) microscope (Peabody). Different sections per sample were imaged.

2.5 | Flow cytometry

A volume of 9 mL at a concentration of 70×10^4 B16 F10 and RAW 264.7 cells/mL was plated in a T75 cm^2 tissue culture flask (6.3×10^6 cells/flask). After allowing for attachment, cells were treated as previously described at stated IC_{50} values. Cells were harvested, centrifuged at 3000 rpm for 5 min and washed twice with ice-cold PBS. Cells were then fixed in ice-cold 70% methanol (v/v) dropwise while gently vortex mixing and thereafter stored at −20°C until further analysis. On the day of analysis, cells were washed once in 0.5% bovine serum albumin (BSA)/PBS buffer (for flow cytometry, all washes included centrifugation at 3000 rpm for 3 min) before adding the stain or antibody. Additionally, cells were vortexed before analysing them on the Flow Check™ Pro (Beckman Coulter) attached to an air-cooled argon laser.

For all flow cytometry analyses, unstained control cells treated with PBS were used to set positive gates for the cells treated with the kynurenine exogenous compounds. Analysed data was derived from a minimum of 15,000 cells using Kaluza C data analysis software (Version 1.1.00003.20057; Beckman Coulter). Debris and doublets were gated out and, therefore, excluded from further analyses. All flow cytometry data is representative of at least two experimental repeats ($n = 2$) (mean ± standard error of mean [SEM]) and presented as a composite univariate histogram.

2.5.1 | Cell cycle progression

Each sample was supplemented with 500 µL of 0.1 M PBS containing propidium iodide (PI) (40 µg/mL), RNase (100 µg/mL) and 0.1% Triton X-100. Cells were incubated in the dark for 40 min at 37°C and 5% CO_2 in a humidified incubator.

2.5.2 | Protein activation of ERK1/2

Each sample, containing 1,000,000 cells, was supplemented with 5 µL Phos-ERK1 (T202/Y204)/ERK2 (T185/Y187) Alexa Fluor® 488-conjugated antibody from R&D systems (supplied in a saline solution containing BSA and sodium azide) at a concentration of 0.95 µg/mL in sterile PBS, as per the manufacturer's instructions. Samples were incubated for 40 min at 2–8°C. After 40 min, cells were centrifuged and resuspended in 1 mL of 0.5% (w/v) BSA in PBS buffer.

2.5.3 | Apoptosis detection with Annexin V

Flow cytometry was utilised to quantify apoptosis with the dual staining of Annexin V conjugated to a fluorochrome, fluorescein isothiocyanate (FITC) and PI, using the Invitrogen™ ApoDETECT Annexin V-FITC Kit from Thermo Fisher Scientific. Cells were resuspended in 1 mL of 1× binding buffer. Cells in suspension (190 µL) were transferred to microcentrifuge tubes and 10 µL Annexin V-FITC was added. Samples were incubated for 10 min in the dark at room temperature. After 10 min, samples were vortexed, and the supernatant was discarded. Cells were resuspended in 190 µL of 1× binding buffer, and 10 µL of PI was added.

Dot plots for PI (FL3 log) versus dot plots for Annexin V-FITC (FL1 log) were created for B16 F10 and RAW 264.7 cells and can be found in the supplementary files. The data were grouped into four quadrants, each representing a different type of cell death. Cell death was analysed as follows: viable cells in the lower left quadrant, where FITC (−) and PI (−); necrotic cells in the lower right quadrant, where FITC (−) and PI (+); early apoptotic cells in the upper left quadrant where FITC (+) and PI (−) and late apoptotic cells in the upper right quadrant where FITC (+) and PI (+).

2.6 | Statistics

All quantitative data was represented as mean ± SEM. Flow cytometry experiments were conducted twice and tested for significant differences using an analysis of variance, with Tukey post hoc analysis where $p \leq .05$ was considered significant. The statistical programme GraphPad Prism was used for statistical analyses. For all statistical analyses, kynurenine exogenous compounds were compared to the control cells treated with 0.1 M PBS, whereas NOC-treated cells were compared to the control cells treated with ddH_2O.

3 | RESULTS

3.1 | Transmission electron microscopy

A summary of the intracellular morphological changes is included in the Supporting Information files.

The PBS and ddH_2O control samples of B16 F10 and RAW 264.7 cells (Figure 1a–h), presented with intact nuclei and nucleoli, while the rough endoplasmic reticulum (RER) as well as the mitochondria remained unaffected. B16 F10 cells exposed to L-kyn at 1.74 mM for 48 h

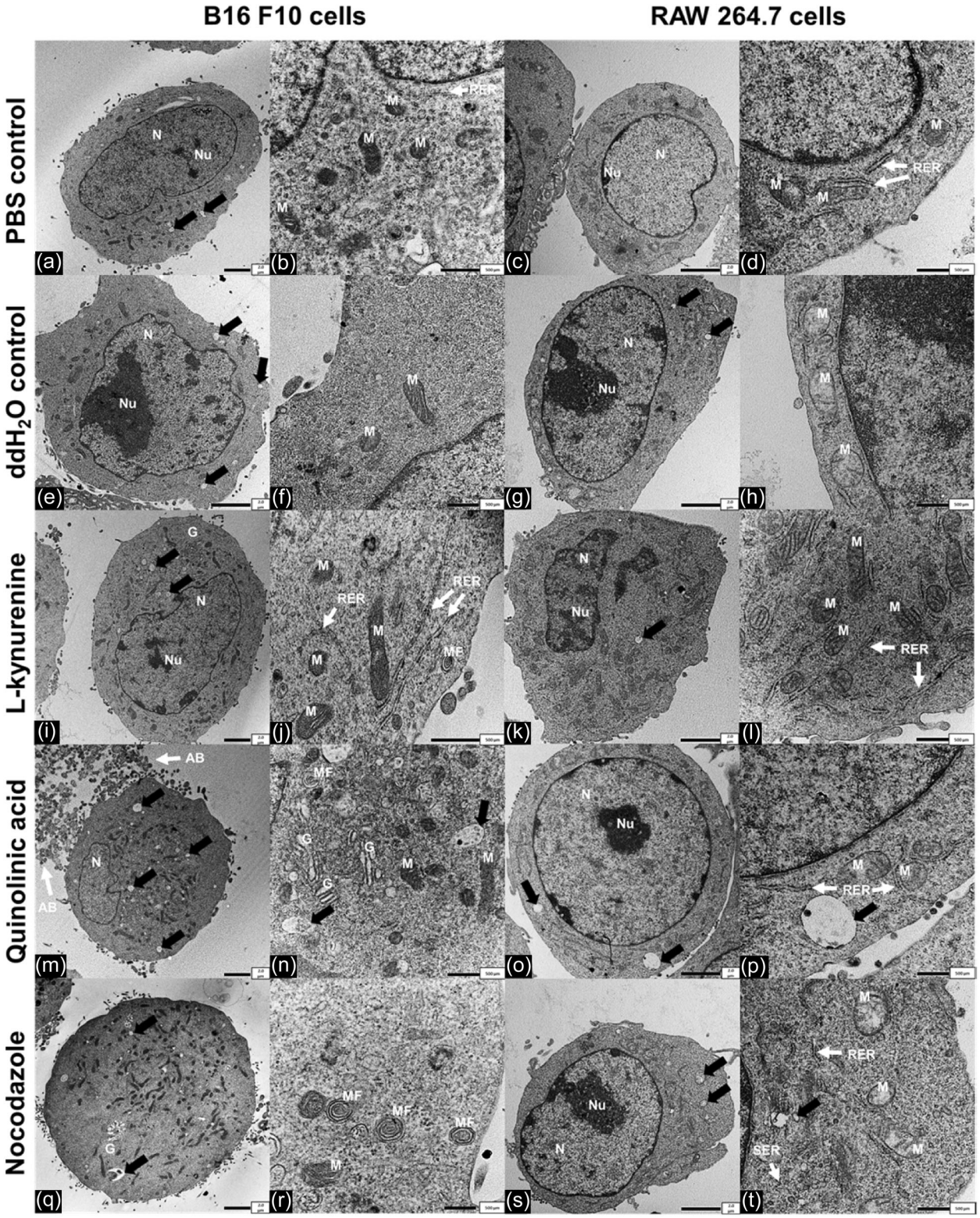

FIGURE 1 Transmission electron micrographs of B16 F10 and RAW 264.7 cells at 48 h after exposure to phosphate-buffered saline (a–d), ddH_20 (e–h), L-kyn at 1.74 mM (i–l), Quin at 8.23 mM (m–p) and NOC at 1.30 Mm (q–t). The scale bar at the bottom right corner represents 2 μm at ×3000 magnification and 500 μm at ×10,000 magnification. Red arrows indicate lysosomes and vacuoles; white arrows indicate mitochondria; orange arrows indicate the nucleus; blue arrows indicate nucleolus; purple arrows indicate rough endoplasmic reticulum; pink arrows indicate myelin figures. Black arrows indicate lysosomes and vacuoles. AB, apoptotic bodies; G, Golgi complex; M, Mitochondria; MF, Myelin Figure; N, nucleus; Nu, nucleolus; RER, rough endoplasmic reticulum; SER, smooth endoplasmic reticulum.

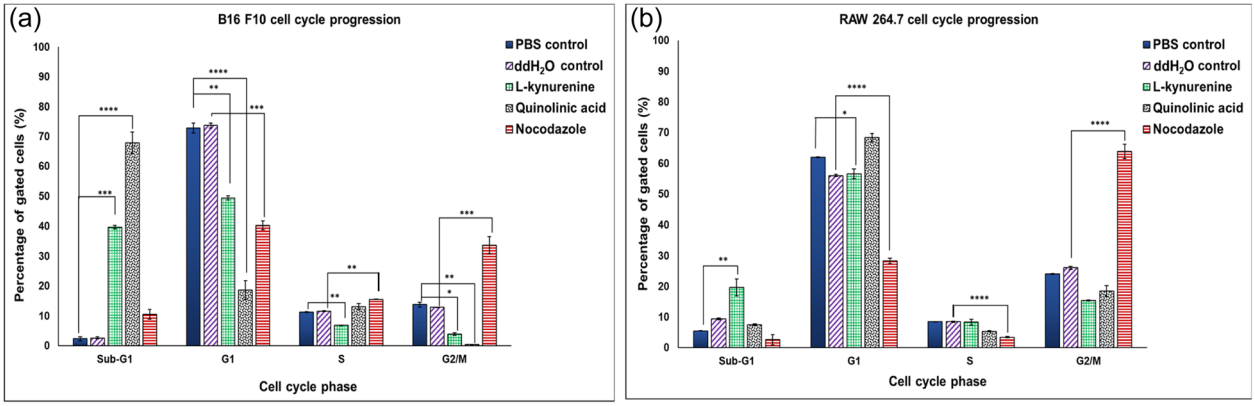

FIGURE 2 Quantitative representation of the percentage gated B16 F10 (a) and RAW 264.7 (b) cells in the different phases of the cell cycle (sub-G1, G1, S and G2/M) after 48 h for control cells treated with phosphate-buffered saline (PBS), control cells treated with ddH_2O, L-kyn-treated cells at 1.74 mM, Quin-treated cells at 8.23 mM and positive control cells treated with nocodazole at 1.30 mM. The bar graphs represent the average of at least two experimental repeats, with the standard error of mean indicated by the error bars. $^*p \le .05$; $^{**}p \le .01$; $^{***}p \le .001$ indicates a significant difference compared to the control treated with PBS or ddH_2O.

presented with clearly defined nuclei and nucleoli (Figure 1i,j) and the RER as well as the mitochondria remained unaffected. Some lysosomes and vacuoles were present (black arrows) but were not increased compared to the control cells. However, the Golgi complex appeared swollen, and some myelin figures were present. Similar to the PBS and ddH_2O control cells, L-kyn-treated RAW 264.7 cells (Figure 1k,l) presented with clearly defined nuclei and nucleoli and unaffected organelles. In B16 F10 cells treated with Quin at 8.23 mM for 48 h (Figure 1m,n), the nuclei in cells were clearly defined. B16 F10 cells Quin-treated cells presented with an increased amount of lysosomes and vacuoles (black arrows) as well as apoptotic bodies, while the RER and the mitochondria remained unaffected. Golgi complexes appeared swollen, and some myelin figures were present. Quin-treated RAW 264.7 cells (Figure 1o,p) presented with lysosomes and vacuoles. NOC-treated B16 F10 cells (Figure 1q,r) appeared rounded with absent nuclei and nucleoli in the majority of the cells. Additionally, myelin figures were present and Golgi complexes swollen. NOC-treated RAW 264.7 cells (Figure 1s,t) presented with membrane blebbing, an increased amount of lysosomes and vacuoles, swollen mitochondria and swollen smooth endoplasmic reticulum.

3.2 | Cell cycle progression

Flow cytometry histograms and a table summary for the B16 F10 and RAW 264.7 cell lines are included in the supplementary files. Figure 2a,b demonstrate the quantitative representation of the percentage gated B16 F10 and RAW 264.7 cells in the different phases of the cell cycle.

For the B16 F10 cell line, the ddH_2O-treated control cells did not display any significant effects compared to the PBS-treated control cells. L-kyn exposure induced an accumulation of cells in the sub-G1 phase (39.68 ± 0.63) as well as a decrease in cells occupying the G1 (49.40 ± 0.71), S (6.92 ± 0.02) and G2/M (3.87 ± 0.40) phase (Figure 2a). The treatment of B16 F10 cells with Quin resulted in an accumulation of cells in the sub-G1 phase (67.91 ± 3.63) as well as a decrease in cells occupying the G1 (18.58 ± 3.14) and G2/M (0.39 ± 0.06) phase (Figure 2a). NOC exposure led to a decrease in cells occupying the G1 phase (40.29 ± 1.51) as well as an increase in cells in the S (15.52 ± 0.08) and G2/M (33.65 ± 2.91) phase (Figure 2a).

In RAW 264.7 cells, the ddH_2O-treated control cells did not display any significant effects compared to the PBS-treated control cells. L-kyn displayed a significant increase in cells occupying the sub-G1 phase (19.64 ± 2.72) and displayed a decreased cell population in the G1 (56.53 ± 1.60) (Figure 2b). Quin did not cause significant changes in the cell cycle distribution (Figure 2b). NOC exposure induced a decrease in cells occupying the G1 phase (28.24 ± 0.88) and the S phase (3.45 ± 0.25) and a significant increase in the G2/M (63.82 ± 2.36) phase (Figure 2b).

3.3 | ERK1/2 activation quantification

Figure 3 demonstrates the quantitative representation of the percentage gated B16 F10 and RAW 264.7 cells that activate ERK1/2. For the B16 F10 cell line, both L-kyn (11.56 ± 1.04) and Quin (28.23 ± 2.72) exposure significantly inhibited ERK1/2 activation (Figure 3). NOC exposure significantly inhibited ERK1/2 activation (72.44 ± 1.63) (Figure 3). The RAW 264.7 cell line did not activate ERK1/2, and neither L-kyn, Quin nor NOC significantly affected the activation of ERK1/2 in the RAW 264.7 cell line (Figure 3).

3.4 | Cell death

For the B16 F10 cell line, the ddH_2O-treated control cells did not display any significant effects compared to the PBS-treated control cells. L-kyn exposure induced a decrease in the viable cell population (9.39 ± 1.20) as well as an increase in the necrotic population

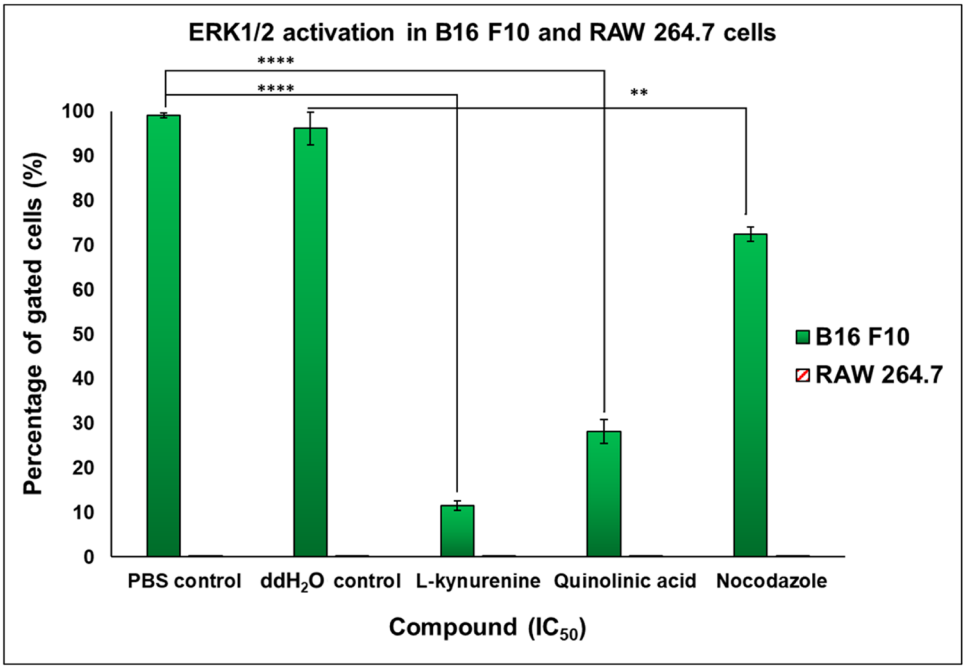

FIGURE 3 Quantitative representation of extracellular signal-regulated kinase 1/2 (ERK1/2) activation in B16 F10 cells and RAW 264.7 cells after 48 h for control cells treated with phosphate-buffered saline (PBS), control cells treated with ddH_2O, L-kyn-treated cells at 1.74 mM, Quin acid-treated cells at 8.23 mM, positive control cells treated with nocodazole at 1.30 mM. The bar graphs represent the average of at least two experimental repeats, with the standard error of mean indicated by the error bars. $^{**}p \leq .01$; $^{****}p \leq .0001$ indicates a significant difference compared to the control cells treated with PBS or ddH_2O.

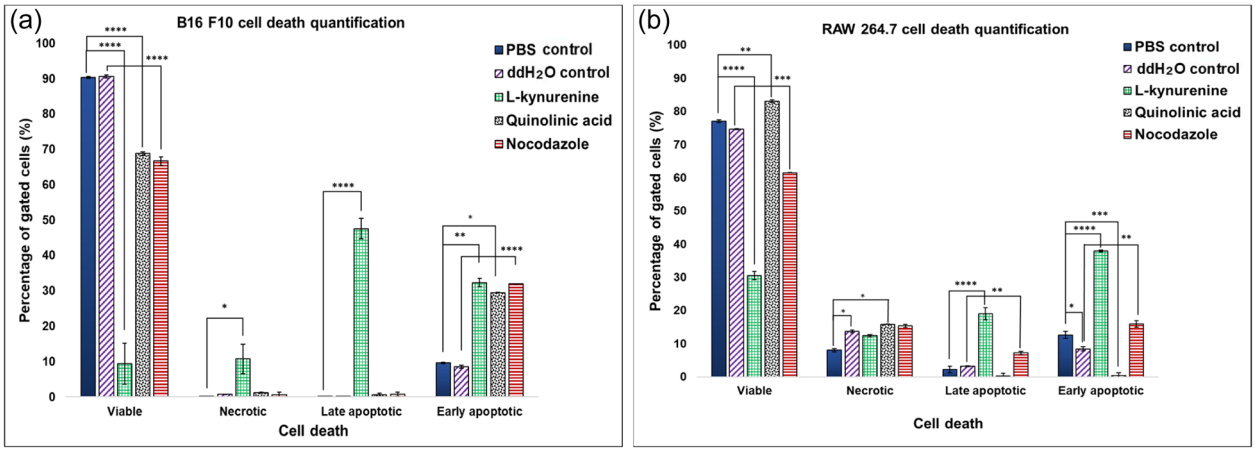

FIGURE 4 Quantitative representation of cell death in B16 F10 (a) and RAW 264.7 (b) cells after 48 h for control cells treated with phosphate-buffered saline (PBS), control cells treated with ddH_2O, L-kyn-treated cells at 1.74 mM, Quin-treated cells at 8.23 mM and positive control cells treated with nocodazole at 1.30 mM. The bar graphs represent the average of at least two experimental repeats, with the standard error of mean indicated by the error bars. $^{*}p \leq .05$; $^{**}p \leq .01$; $^{****}p \leq .0001$ indicates a significant difference compared to the control treated with PBS or ddH_2O.

(10.73 ± 2.85), the early apoptotic population (32.30 ± 5.79) and late apoptotic cell population (47.58 ± 4.14). The treatment of B16 F10 cells with Quin resulted in a decrease in the viable cell population (68.83 ± 0.09) as well as an increase in the early apoptotic cell population (29.48 ± 0.51) (Figure 4a). NOC exposure led to a decrease in viable cells (66.73 ± 0.02) as well as an increase in cells in the early apoptotic stage (Figure 4a).

For the RAW 264.7 cell line, the ddH_2O-treated control cells displayed a slightly lower percentage of cells in the early apoptotic phase (74.68 ± 0.18) ($p = .02$), as well as a slight increase in necrotic cells ($p = .05$) in comparison to the PBS-treated control cells (77.10 ± 0.43). L-kyn exposure induced a decrease in the viable population (30.51 ± 1.23) as well as an increase in the late apoptotic population (19.04 ± 1.86) and early apoptotic population (38.01 ± 0.28) (Figure 4b). Interestingly,

the treatment of RAW 264.7 cells with Quin resulted in a slight increase in the viable cell population (83.07 ± 0.36) and the necrotic cell population (15.88 ± 0.06), as well as a decrease in the early apoptotic cell population (0.43 ± 0.78) (Figure 4b). NOC exposure led to a decrease in viable cells (61.51 ± 0.05) as well as an increase in cells in the late apoptotic stage (7.22 ± 0.46) and early apoptotic stage (15.95 ± 1.01) (Figure 4b).

4 | DISCUSSION

In a prior investigation, the authors investigated the cytotoxicity and morphological changes induced by L-kyn, Quin and kynurenic acid (KA) on B16 F10, RAW 264.7 and HaCat cells at 24, 48 and 72 h, spanning concentrations from 0 to 5 mM. The current study tested L-kyn and Quin at these previously determined 48-h IC_{50} values on B16 F10 and RAW 264.7 cells (Basson et al., 2023b), which both express all the kynurenine enzymes (Guillemin et al., 2003). This current study found that (1) L-kyn and Quin each displayed different effects in terms of intracellular morphological changes, cell cycle progression, cell death and ERK1/2 inhibition and (2) that both L-kyn and Quin displayed different effects in different cell lines (B16 F10 compared to RAW 264.7 cells). These factors may be explained by the fact that different metabolites in the kynurenine pathway act as active substances, where each metabolite exerts different effects on different cell populations despite its common origin (Austin & Rendina, 2015; Moffett & Namboodiri, 2003). Therefore, L-kyn, which is an Ahr agonist (Walczak et al., 2020a), may exert different effects than Quin, which is a *N*-methyl-D-aspartate type glutamate receptors agonist (Nkandeu et al., 2022).

First, TEM was used to observe intracellular morphological changes induced by kynurenine compounds on B16 F10 and RAW 264.7 cells, as TEM is the gold standard to confirm apoptosis (Elmore, 2007). Both L-kyn and Quin induced swelling of the Golgi apparatus in B16 F10 cells but not in RAW 264.7 cells. A previous study by Bottone et al. indicated that morphological changes of the Golgi apparatus, including fragmentation, distension and swelling, can occur under apoptotic conditions (Bottone et al., 2013). Furthermore, L-kyn and Quin induced the formation of myelin figures in B16 F10 cells, but not in RAW 264.7 cells. A previous study suggested that these myelin figures may be derived from cell membranes that coil into whorls during reversible cell injury, but become more prominent in irreversibly injured cells (Miller & Zachary, 2017). A previous study investigating the cytotoxic oxysterols (7KC, 7β-OH and 5β, 6β-epoxide), concluded that myelin figure formation occurred independently of caspase activation (Vejux et al., 2007). Wilkonson elucidated that the emergence of whorls may be a consequence of autophagy induced by endoplasmic reticulum stress (Wilkinson, 2019). Previous evidence indicated that Quin induced striatal neuron death, through both apoptotic and autophagic mechanisms, induced by nuclear factor kappa B and p53 (Lugo-Huitrón et al., 2013). Furthermore, this study demonstrated that Quin induced an increased amount of lysosomes and vacuoles in both cell lines, which has previously been linked to cell death (Appelqvist et al., 2013), such as autophagy (Salazar et al., 2011). These considerations suggested that some relationships may exist between kynurenine compounds, cell death and myelin figure formation and that future studies should investigate the effects of kynurenine compounds on different types of cell death and the possible crosstalk between apoptosis and autophagy.

The cell cycle is regarded as an important determinant of cancer progression, as cell cycle checkpoint disruption is implicated in cancer progression, leading to uncontrolled proliferation and resistance to apoptotic cell death (Visconti et al., 2016). A previous study demonstrated the apoptotic effects of L-kyn on natural killer cells, demonstrating its effect in immune escape. Notably, the observed apoptotic effects did not manifest through cell cycle arrest, despite a marginal elevation of cells in the G0/G1 phase (Song et al., 2011). Data from this study indicated that treatment of B16 F10 cells with L-kyn and Quin resulted in a significant increase in cells occupying the sub-G1 phase of the cell cycle, indicating the initiation of apoptosis as apoptotic cells have lower DNA sustainability (Darzynkiewicz et al., 1992). In addition, a decreased amount of cells resided in the G2/M phase, indicating that cells did not enter the mitotic phase due to irreparable DNA damage (Hayashi & Karlseder, 2013). These changes were accompanied by a significant decrease in the G1 phase, indicating a reduction in cell growth. However, these changes were less significant in the RAW 264.7 cells. This may indicate that one of the mechanisms by which L-kyn and Quin may act to inhibit the proliferation of B16 F10 melanoma cells is through the inhibition of cell cycle progression.

Another important marker of cell proliferation is ERK1/2, which belongs to the MAP-K family (Guo et al., 2020) and is upregulated in up to 80% of melanomas (Nkandeu et al., 2022). Our results indicate that both L-kyn and Quin significantly inhibited ERK1/2 activation in B16 F10 cells and that L-kyn inhibited ERK1/2 activation in B16 F10 melanoma cells to a greater extent than Quin. This is in alignment with a recent study, indicating that L-kyn (an Ahr agonist) was the most potent cytotoxic kynurenine metabolite towards B16 F10 melanoma cells (Basson et al., 2023b). These results are supported by a previous study where KA (another Ahr agonist in the kynurenine pathway) activated GPR35, leading to the inhibition of phosphorylation of various signalling proteins, such as Akt, ERK and p38 mitogen-activated protein kinase (p38). However, the specific study did not investigate the effects of L-kyn and Quin on these signalling pathways. Furthermore, the study suggested that KA may alter proliferation, cell cycle, cell survival and migration through the disruption of the phosphoinositide 3-kinase/protein kinase B PI3K/Akt pathway as well as differentiation, proliferation or apoptosis through the disruption of the ERK pathway (Walczak et al., 2020b).

In the current study, however, ERK1/2 was not activated in RAW 264.7 cells. Therefore, the authors suggest that the level of expression and activation of these receptors may differ between B16 F10 and RAW 264.7 cell lines, thus giving rise to the differences in the mechanism of the effects observed. In addition, a previous study reported that ERK1/2 activation leads to the phosphorylation and subsequent activation of numerous signalling molecules in the MAP-K pathway, which regulate cell processes, such as cell cycle progression, differentiation and survival (Sugiura et al., 2021).

Therefore, the inhibition of ERK1/2 is an important antitumour strategy for melanoma (Zhuang, 2005). Ongoing activation of the ERK MAPK-K pathway can transform normal cells into tumour cells, where the inhibition of the ERK MAP-K pathway can inhibit tumour growth (Sugiura et al., 2021). In addition to the correlation between ERK1/2 and tumour growth, ERK1/2 is one of the most important role players in tumour metastasis (Zhuang, 2005), which may indicate the potential antimetastatic properties of L-kyn and Quin. Huang et al. found that the inhibition of the ERK/MAP-K pathway in lymphoma cells suppressed cell proliferation and promoted apoptosis (Huang et al., 2019).

In support of the cell cycle, morphological and ERK1/2 activation results, it was found that L-kyn reduced viable cells and induced cell death, namely necrosis, early and late apoptosis in B16 F10 cells, but only early and late apoptosis in RAW 264.7 cells. Finding that L-kyn induces both early and late apoptosis can be explained by the fact that the loss of the membrane integrity is a gradual process. The cell membrane of early apoptotic cells is thus still intact and impermeable to PI. If these apoptotic cells are not successfully removed by macrophage-mediated phagocytosis, cells will progress to the late apoptotic phase, where the cell membrane integrity is compromised and thus permeable to PI (Kari et al., 2022). The controversy regarding AhR activation in tumour apoptosis is reflected in the literature, as one study indicated that L-kyn suppressed apoptosis in P20E breast cancer cells (Bekki et al., 2015), while another found that the exogenous treatment of A375 melanoma cells with L-kyn induced necrosis, but not apoptosis (Walczak et al., 2020a). In the current study, Quin also caused a reduction in viable B16 F10 melanoma cells, while inducing early apoptosis. However, early apoptosis was suppressed in Quin-treated RAW 264.7 cells and instead led to an increase in necrosis. Necrosis is a significant contributor to inflammation due to the release of intracellular substances, which may be detrimental to surrounding cells (Yang et al., 2015). Therefore, this warrants further research to elaborate on the effects of Quin on other noncancerous cell lines as it may be potentially toxic to surrounding cells.

In conclusion, this study provides a better understanding of the in vitro therapeutic effects of L-kyn and Quin against B16 F10 melanoma cells and confirms that both of these kynurenine metabolites exert a different mechanism of action, which is cell line dependent. Furthermore, kynurenine compounds inhibited B16 F10 cell proliferation and survival through ERK1/2 activation inhibition, cell cycle alterations, cell death and intracellular morphological changes, with less pronounced effects in the noncancerous RAW 264.7 macrophage cell line. However, these findings need to be substantiated with additional cell lines.

AUTHOR CONTRIBUTIONS

All experiments and data analyses were conducted by Charlise Basson. Charlise Basson, Yvette Nkondo Hlophe, June Cheptoo Serem and Priyesh Bipath contributed to data interpretation. Charlise Basson wrote the original draft with critical review and input from Priyesh Bipath, YH and June Cheptoo Serem. YH and Priyesh Bipath contributed to the study's conception and design. All authors gave final approval for the manuscript and are accountable for ensuring accuracy of all aspects of the work.

ACKNOWLEDGEMENTS

The authors would like to acknowledge Antoinette Lensink and Danielle Henn at the University of Pretoria Veterinary Science Electron Microscopy (EM) Unit. The author(s) disclosed receipt of the following financial support for the research, authorship and/or publication of this article: The Research Development programme of Dr Y. N. Hlophe and Dr J. C. Serem by the University of Pretoria. University of Pretoria, Physiology Head of Department, Prof A. Joubert for funding to present this work at a national congress. Struwig/Germeshuysen Kankernavorsingstrust and School of Medicine Research Committee (RESCOM) Grant awarded to Ms Basson. National Research Foundation (NRF) awarded to Prof R. Anguelov.

CONFLICT OF INTEREST STATEMENT

The authors declare no conflict of interest.

DATA AVAILABILITY STATEMENT

The data that support the findings of this study are available from the corresponding author upon reasonable request.

ETHICS APPROVAL STATEMENT

The ethical consent for this study was obtained from the University of Pretoria, Faculty of Health Science, Research Ethics Committee (reference number: 405/2020).

ORCID

Charlise Basson http://orcid.org/0000-0002-6123-9707
June Cheptoo Serem http://orcid.org/0000-0001-9912-166X
Priyesh Bipath http://orcid.org/0000-0002-5433-7069
Yvette Nkondo Hlophe http://orcid.org/0000-0002-3112-2436

REFERENCES

Appelqvist, H., Wäster, P., Kågedal, K., & Öllinger, K. (2013). The lysosome: From waste bag to potential therapeutic target. *Journal of Molecular Cell Biology*, *5*, 214–226.

Austin, C. J. D., & Rendina, L. M. (2015). Targeting key dioxygenases in tryptophan-kynurenine metabolism for immunomodulation and cancer chemotherapy. *Drug Discovery Today*, *20*, 609–617.

Basson, C., Serem, J. C., Hlophe, Y. N., & Bipath, P. (2023a). The tryptophan–kynurenine pathway in immunomodulation and cancer metastasis. *Cancer Medicine*, *18*, 18691–18701.

Basson, C., Serem, J. C., Hlophe, Y. N., & Bipath, P. (2023b). An in vitro investigation of l-kynurenine, quinolinic acid, and kynurenic acid on B16 F10 melanoma cell cytotoxicity and morphology. *Cell Biochemistry and Function*, *7*, 912–922.

Bekki, K., Vogel, H., Li, W., Ito, T., Sweeney, C., Haarmann-Stemmann, T., Matsumura, F., & Vogel, C. F. A. (2015). The aryl hydrocarbon receptor (AhR) mediates resistance to apoptosis induced in breast cancer cells. *Pesticide Biochemistry and Physiology*, *120*, 5–13.

Bottone, M., Santin, G., Aredia, F., Bernocchi, G., Pellicciari, C., & Scovassi, A. (2013). Morphological features of organelles during apoptosis: An overview. *Cells*, *2*, 294–305.

Bungsu, I., Kifli, N., Ahmad, S. R., Ghani, H., & Cunningham, A. C. (2021). Herbal plants: The role of AhR in mediating immunomodulation. *Frontiers in Immunology*, *12*, 697663.

Darzynkiewicz, Z., Bruno, S., Del Bino, G., Gorczyca, W., Hotz, M. A., Lassota, P., & Traganos, F. (1992). Features of apoptotic cells measured by flow cytometry. *Cytometry*, *13*, 795–808.

Davis, L. E., Shalin, S. C., & Tackett, A. J. (2019). Current state of melanoma diagnosis and treatment. *Cancer Biology & Therapy*, *20*, 1366–1379.

Dhanyamraju, P. K., & Patel, T. N. (2022). Melanoma therapeutics: A literature review. *The Journal of Biomedical Research*, *36*, 77–97.

Domingues, B., Lopes, J., Soares, P., & Populo, H. (2018). Melanoma treatment in review. *ImmunoTargets and Therapy*, *7*, 35–49.

Elmore, S. (2007). Apoptosis: A review of programmed cell death. *Toxicologic Pathology*, *35*, 495–516.

Guan, M., Zhu, S., & Li, S. (2021). Recent progress in nanomedicine for melanoma theranostics with emphasis on combination therapy. *Frontiers in Bioengineering and Biotechnology*, *9*. https://doi.org/10.3389/fbioe.2021.661214

Guillemin, G. J., Smith, D. G., Smythe, G. A., Armati, P. J., & Brew, B. J. (2003). Expression of the kynurenine pathway enzymes in human microglia and macrophages. *Advances in Experimental Medicine and Biology*, *527*, 105–112.

Guo, Y. J., Pan, W. W., Liu, S. B., Shen, Z. F., Xu, Y., & Hu, L. L. (2020). ERK/MAPK signalling pathway and tumorigenesis. *Experimental and Therapeutic Medicine*, *19*, 1997–2007.

Hanahan, D., & Weinberg, R. A. (2011). Hallmarks of cancer: The next generation. *Cell*, *144*, 646–674.

Hayashi, M. T., & Karlseder, J. (2013). DNA damage associated with mitosis and cytokinesis failure. *Oncogene*, *32*, 4593–4601.

Huang, Y., Zou, Y., Lin, L., Ma, X., & Zheng, R. (2019). miR-101 regulates the cell proliferation and apoptosis in diffuse large B-cell lymphoma by targeting MEK1 via regulation of the ERK/MAPK signaling pathway. *Oncology Reports*, *41*, 377–386.

Kari, S., Subramanian, K., Altomonte, I. A., Murugesan, A., Yli-Harja, O., & Kandhavelu, M. (2022). Programmed cell death detection methods: A systematic review and a categorical comparison. *Apoptosis*, *27*, 482–508.

Leonardi, G., Falzone, L., Salemi, R., Zanghì, A., Spandidos, D., McCubrey, J., Candido, S., & Libra, M. (2018). Cutaneous melanoma: From pathogenesis to therapy (Review). *International Journal of Oncology*, *52*, 1071–1080.

Lugo-Huitrón, R., Ugalde Muñiz, P., Pineda, B., Pedraza-Chaverrí, J., Ríos, C., & Pérez-de la Cruz, V. (2013). Quinolinic acid: An endogenous neurotoxin with multiple targets. *Oxidative Medicine and Cellular Longevity*, *2013*, 1–14.

Macchiarulo, A., Camaioni, E., Nuti, R., & Pellicciari, R. (2009). Highlights at the gate of tryptophan catabolism: A review on the mechanisms of activation and regulation of indoleamine 2,3-dioxygenase (IDO), a novel target in cancer disease. *Amino Acids*, *37*, 219–229.

Mehmel, M., Jovanović, N., & Spitz, U. (2020). Nicotinamide riboside–The current state of research and therapeutic uses. *Nutrients*, *12*, 1616.

Miller, M. A., & Zachary, J. F. (2017). Mechanisms and morphology of cellular injury, adaptation, and death. *Pathologic Basis of Veterinary Disease*, 2–43.e19. https://doi.org/10.1016/B978-0-323-35775-3.00001-1

Moffett, J. R., Arun, P., Puthillathu, N., Vengilote, R., Ives, J. A., Badawy, A. A. B., & Namboodiri, A. M. (2020). Quinolinate as a marker for kynurenine metabolite formation and the unresolved question of NAD(+) synthesis during inflammation and infection. *Frontiers in Immunology*, *11*, 31.

Moffett, J. R., & Namboodiri, M. A. (2003). Tryptophan and the immune response. *Immunology & Cell Biology*, *81*, 247–265.

Navas, L. E., & Carnero, A. (2021). NAD+ metabolism, stemness, the immune response, and cancer. *Signal Transduction and Targeted Therapy*, *6*, 2.

Nkandeu, D. S., Basson, C., Joubert, A. M., Serem, J. C., Bipath, P., Nyakudya, T., & Hlophe, Y. (2022). The involvement of a chemokine receptor antagonist CTCE-9908 and kynurenine metabolites in cancer development. *Cell Biochemistry and Function*, *40*, 608–622.

Rebecca, V. W., Somasundaram, R., & Herlyn, M. (2020). Pre-clinical modeling of cutaneous melanoma. *Nature Communications*, *11*, 2858.

Salazar, M., Hernández-Tiedra, S., Torres, S., Lorente, M., Guzmán, M., & Velasco, G. (2011). Chapter Seventeen–Detecting autophagy in response to ER stress signals in cancer. In P. M. Conn, *Methods in enzymology* (pp. 297–317). Academic Press.

Sever, R., & Brugge, J. S. (2015). Signal transduction in cancer. *Cold Spring Harbor Perspectives in Medicine*, *5*, a006098.

Song, H., Park, H., Kim, Y.-S., Kim, K. D., Lee, H.-K., Cho, D.-H., Yang, J. W., & Hur, D. Y. (2011). L-kynurenine-induced apoptosis in human NK cells is mediated by reactive oxygen species. *International Immunopharmacology*, *11*, 932–938.

Sugiura, R., Satoh, R., & Takasaki, T. (2021). ERK: A double-edged sword in cancer. ERK-dependent apoptosis as a potential therapeutic strategy for cancer. *Cells*, *10*, 2509.

Vejux, A., Kahn, E., Ménétrier, F., Montange, T., Lherminier, J., Riedinger, J. M., & Lizard, G. (2007). Cytotoxic oxysterols induce caspase-independent myelin figure formation and caspase-dependent polar lipid accumulation. *Histochemistry and Cell Biology*, *127*, 609–624.

Visconti, R., Della Monica, R., & Grieco, D. (2016). Cell cycle checkpoint in cancer: A therapeutically targetable double-edged sword. *Journal of Experimental & Clinical Cancer Research*, *35*, 153.

Walczak, K., Langner, E., Makuch-Kocka, A., Szelest, M., Szalast, K., Marciniak, S., & Plech, T. (2020). Effect of tryptophan-derived AhR ligands, kynurenine, kynurenic acid and FICZ, on proliferation, cell cycle regulation and cell death of melanoma cells-in vitro studies. *International Journal of Molecular Sciences*, *21*(21), 7946. https://doi.org/10.3390/ijms21217946

Walczak, K., Wnorowski, A., Turski, W. A., & Plech, T. (2020). Kynurenic acid and cancer: facts and controversies. *Cellular and Molecular Life Science*, *77*, 1531–1550.

Wilkinson, S. (2019). ER-phagy: Shaping up and destressing the endoplasmic reticulum. *FEBS Journal*, *14*, 2645–2763.

Yang, Y., Jiang, G., Zhang, P., & Fan, J. (2015). Programmed cell death and its role in inflammation. *Military Medical Research*, *2*, 12.

Zhivotovsky, B., & Orrenius, S. (2010). Cell cycle and cell death in disease: Past, present and future. *Journal of Internal Medicine*, *268*, 395–409.

Zhuang, L. (2005). Activation of the extracellular signal regulated kinase (ERK) pathway in human melanoma. *Journal of Clinical Pathology*, *58*, 1163–1169.

van Zijl, F., Krupitza, G., & Mikulits, W. (2011). Initial steps of metastasis: Cell invasion and endothelial transmigration. *Mutation Research/Reviews in Mutation Research*, *728*, 23–34.

SUPPORTING INFORMATION

Additional supporting information can be found online in the Supporting Information section at the end of this article.

How to cite this article: Basson, C., Serem, J. C., Bipath, P., & Hlophe, Y. N. (2024). L-kynurenine and quinolinic acid inhibited markers of cell survival in B16 F10 melanoma cells in vitro. *Cell Biology International*, *48*, 964–972. https://doi.org/10.1002/cbin.12163